08 Feb 2022

Epitaxial Electrodeposition of Hole Transport CuSCN Nanorods on Au(111) at the Wafer Scale and Lift-Off to Produce Flexible and Transparent Foils

Bin Luo

Avishek Banik

Eric W. Bohannan
Missouri University of Science and Technology, bohannan@mst.edu

Jay A. Switzer
Missouri University of Science and Technology, jswitzer@mst.edu

Recommended Citation

B. Luo et al., "Epitaxial Electrodeposition of Hole Transport CuSCN Nanorods on Au(111) at the Wafer Scale and Lift-Off to Produce Flexible and Transparent Foils," *Chemistry of Materials*, vol. 34, no. 3, pp. 970 - 978, American Chemical Society, Feb 2022.
The definitive version is available at https://doi.org/10.1021/acs.chemmater.1c02694

CHEMISTRY OF MATERIALS

pubs.acs.org/cm

Article

Epitaxial Electrodeposition of Hole Transport CuSCN Nanorods on Au(111) at the Wafer Scale and Lift-off to Produce Flexible and Transparent Foils

Bin Luo, Avishek Banik, Eric W. Bohannan, and Jay A. Switzer*

Cite This: *Chem. Mater.* 2022, 34, 970–978

Read Online

ACCESS | Metrics & More | Article Recommendations | Supporting Information

ABSTRACT: The wide bandgap p-type metal pseudohalide semiconductor copper(I) thiocyanate (CuSCN) can serve as a transparent hole transport layer in various opto-electronic applications such as perovsksite and organic solar cells and light-emitting diodes. The material deposits as one-dimensional CuSCN nanorod arrays, which are advantageous due to their high surface area and good charge transport properties. However, the growth of high-quality epitaxial CuSCN nanorods has remained a challenge. Here, we introduce a low cost and highly scalable room temperature procedure for producing epitaxial CuSCN nanorods on Au(111) by an electrochemical method. Epitaxial CuSCN grows on Au(111) with a high degree of in-plane as well as out-of-plane order with +0.22% coincidence site lattice mismatch. The phase of CuSCN that deposits is a function of the Cu^{2+}/SCN^- ratio in the deposition bath. A pure rhombohedral material deposits at higher SCN^- concentrations, whereas a mixture of rhombohedral and hexagonal phases deposits at lower SCN^- concentrations. A Au/epitaxial CuSCN/Ag diode has a diode quality factor of 1.4, whereas a diode produced with polycrystalline CuSCN has a diode quality factor of 2.1. A highly ordered foil of CuSCN was produced by epitaxial lift-off following a triiodide etch of the thin Au substrate. The 400 nm-thick CuSCN foil had an average 94% transmittance in the visible range and a 3.85 eV direct bandgap.

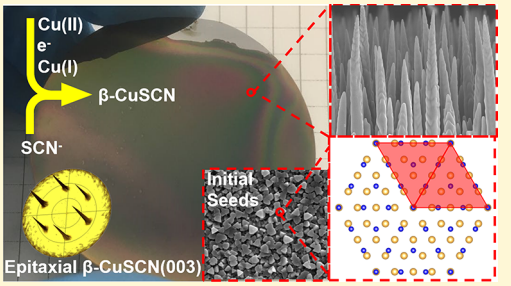

INTRODUCTION

Hole transport materials (HTMs) are essential for opto-electronic devices, such as perovskite solar cells and light-emitting diodes.[1−3] CuSCN is a nontoxic, earth-abundant, wide bandgap (3.7−3.9 eV) p-type metal pseudohalide semiconductor. CuSCN has been steadily gaining attention as a versatile inorganic HTM in stabilized highly efficient perovskite solar cells,[4] standalone solar water splitting devices,[5] light-emitting diodes,[6−8] and transistors.[9−11] The basis for the success of CuSCN as an excellent HTM could be attributed to its exceptional optical transparency, chemical stability, processing versatility, and good hole transport properties.[12] One-dimensional CuSCN nanorod arrays have further attracted attention due to their high surface area and good charge transport properties.[13−15] However, the epitaxial growth of CuSCN nanorods with high out-of-plane as well as in-plane order has remained a challenge. Although CuSCN films have been prepared by various solution processes such as spin coating,[16] electrodeposition,[17−19] and SILAR methods,[20] the deposited CuSCN is a polycrystalline film[21−24] or a film with a fiber texture with no in-plane order,[25,26] limiting its hole transport property. Charge carrier transport across the CuSCN layer is affected by grain boundaries and the crystalline orientation, which would especially impact in-plane transport. The hole mobility (0.01−0.1 $cm^2\ V^{-1}\ s^{-1}$) of solution-processed CuSCN is still quite limited compared with those of other inorganic HTMs.[27−29] A highly ordered hole transport layer provides a low density of defect sites and grain boundaries suppressing charge recombination probabilities and facilitating efficient charge transport.[5] For example, single-crystal spiro-OMeTAD exhibits remarkable mobility, exceeding its thin-film counterparts by three orders of magnitude via mesoscale ordering.[30] In addition, epitaxial hole conducting CuSCN films could serve as substrates for growth of single-crystalline perovskite materials or n-type ZnO layers for high-quality opto-electronic devices.[31] Epitaxial CuSCN also allows for the measurement of electronic properties along specific crystallographic directions. This is especially important for noncubic materials such as CuSCN. Therefore, there is a pressing need to find a method to produce epitaxial CuSCN.

Electrodeposition is a low cost and highly scalable deposition process producing epitaxial metal and semiconductor films.[32−34] Here, we detail an electrochemical method to produce epitaxial CuSCN nanorods on a Au(111)/Si(111) substrate at room temperature from an

Received: August 5, 2021
Revised: December 29, 2021
Published: January 18, 2022

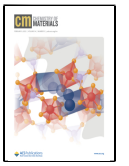

aqueous $CuSO_4$-EDTA-KSCN bath. The material is deposited on a 28 nm-thick layer of Au(111) on a Si(111) wafer that was electrodeposited by a method that we reported earlier.[33] Cu(II) is simply reduced electrochemically in the presence of SCN^- ions. Highly out-of-plane and in-plane ordered nanorods grow from the Au(111) surface with a low CSL mismatch of +0.22%. Two kinds of CuSCN nanorods with a pure rhombohedral phase and mixed rhombohedral/hexagonal phases were produced by adjusting the Cu^{2+}/SCN^- ratio in the deposition bath. Epitaxial CuSCN/Au is an ideal HTM/metal system due to well-aligned work function for ohmic contact and efficient charge transport. However, it faces challenges such as degradation of the CuSCN/Au interface[4] and the limitation of flexibility due to the rigid substrate. Therefore, epitaxial lift-off technology was applied to a flat epitaxial CuSCN film through a simple chemical Au etching with a triiodide ion and a lift-off procedure, which extends the application of highly ordered CuSCN foils to various substrates via a dry-transfer method. This could form the basis of transparent hole transport layers for flexible opto-electronics.[35]

RESULTS AND DISCUSSION

The electrolyte used for the deposition of CuSCN was typically 20 mM $CuSO_4$, 20 mM EDTA, and 80 mM KSCN based on the work by other workers who showed that complexing agents such as EDTA are needed to prevent the precipitation of black $Cu(SCN)_2$, which further decomposes to white CuSCN and thiocyanogen.[18] According to the speciation study of this earlier study, the primary species present in this solution is Cu(II)EDTA with a lower concentration of $CuSCN^+$.[18] Hence, EDTA serves as a reservoir of Cu(II) ions, which keeps the concentration of $CuSCN^+$ low in order to prevent the precipitation/decomposition.

We explored the electrochemistry of deposition using a rotating disk electrode (RDE), which provides well-controlled convection to the electrode surface. Using the RDE, a solution reduction reaction should manifest itself as a mass-tranport-limited plateau with a limiting current that is controlled by the rotation rate, concentration, and diffusion coefficient. Figure 1 shows the linear sweep voltammetry (LSV) analysis results of various electrolytes with a Au RDE at 1000 rpm rotation rate. Figure 1A shows the LSV with a Au RDE in the $CuSO_4$-EDTA-KSCN bath. We observed three cathodic regimes, C1, C2, and C3. The reduction C1 begins at +0.35 V and reaches a plateau with a current density of 1.3 mA/cm^2, indicating a solution species reduction, whereas the reaction at C2 presents itself as a peak, which indicates a surface species reduction that is not mass-transport-limited. We attribute C1 to the reduction of solution $CuSCN^+$ to solid CuSCN, as shown in eq 1.

As shown in Figure 1A, although the range of CuSCN deposition is quite wide, from +0.3 to −0.5 V, epitaxial CuSCN is only achieved using a prepolarized bias of −0.3 to −0.5 V. That is, epitaxial CuSCN is only deposited at potentials negative of the peak at C2. In order to further study the nature of reduction process C2, we predeposited CuSCN to a thickness of approximately 250 nm on the Au RDE at −0.4 V for 60 s and then performed LSV in the $CuSO_4$-EDTA-KSCN bath, as shown in Figure 1B. In this case, C2 is absent, suggesting that C2 is due to the reduction of a surface-adsorbed species on the Au surface. Because the current density at C2 in Figure 1A is higher than that of a self-assembled monolayer, combined with the fact that SCN^- is known to be strongly adsorbed on the Au(111) surface,[37] we

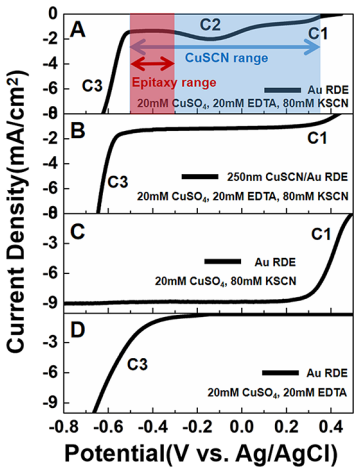

Figure 1. Linear sweep voltammograms (LSVs) of electrolytes with various compositions. (A) Au rotating disk electrode (RDE) in 20 mM $CuSO_4$, 20 mM EDTA, and 80 mM KSCN solution. (B) CuSCN (250 nm)/Au RDE in 20 mM $CuSO_4$, 20 mM EDTA, and 80 mM KSCN solution. 250 nm CuSCN was predeposited at −0.4 V vs Ag/AgCl for 60 s. (C) Au RDE in 20 mM $CuSO_4$ and 80 mM KSCN solution. (D) Au RDE in 20 mM $CuSO_4$ and 20 mM EDTA solution. RDEs were rotated at 1000 rpm. Scan rates of all LSVs were 10 $mV \cdot s^{-1}$.

speculate that C2 is the reduction of an adsorbed Cu-(II)$_x$EDTA$_y$(SCN)$_z$ cluster[18,36,38] on the Au surface that is attached by Au-SCN interaction, as given in eq 2. To understand the effect of EDTA on electrochemistry, we performed LSV using the Au RDE in a $CuSO_4$-KSCN bath without EDTA, as shown in Figure 1C, in which C1 appears as a cathodic plateau with 9 mA/cm^2 that is seven times higher than the $CuSCN^+$ reduction plateau in the $CuSO_4$-EDTA-KSCN bath in Figure 1B. The higher current density for C1 in this bath indicates that EDTA does serve to lower the concentration of $CuSCN^+$ in solution. The voltammogram in this solution lacks reduction process C3, suggesting that C3 in Figure 1A,B is due to the reduction of Cu(II)EDTA to Cu (in eq 3). The deposition solution that does not contain EDTA is not stable for more than a few minutes because of the spontaneous precipitation of CuSCN and $Cu(SCN)_2$ powder, as shown in the typical XRD pattern in Figure S1. Figure 1D shows the LSV of a Au RDE in a solution of 20 mM $CuSO_4$ and 20 mM EDTA (i.e., no SCN^- present). In this case, C1 and C2 are not observed. The only reduction process (C3) is the reduction of Cu(II)EDTA to metallic Cu, as shown in eq 3.

$$Cu(II)SCN^+ + e^- = Cu(I)SCN \quad (1)$$

$$Cu(II)_xEDTA_y(SCN)_z \text{ (adsorbed cluster)} + xe^- = xCuSCN + (z - x)SCN^- + yEDTA \quad (2)$$

$$Cu(II)EDTA + 2e^- = Cu(0) + EDTA \quad (3)$$

Epitaxial CuSCN is only achieved using a prepolarized potential of −0.3 to −0.5 V, as shown in Figure 1A. CuSCN deposited at +0.2 V was analyzed by XRD and SEM, as shown in Figure S3. It is polycrystalline with a slight [001] preferred orientation in the XRD pattern (Figure S3A) and a disordered microstructure (Figure S3B,C). The RDE studies in Figure 1 may provide some insights into why the epitaxial CuSCN can only be produced at potentials negative of C2 in Figure 1A.

https://doi.org/10.1021/acs.chemmater.1c02694
Chem. Mater. 2022, 34, 970−978

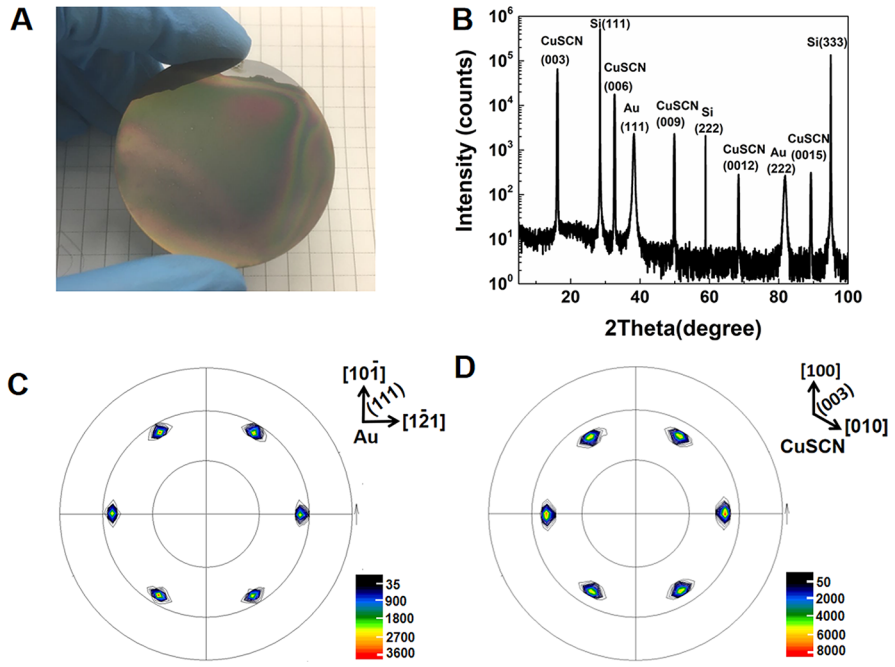

Figure 2. X-ray diffraction pattern and pole figures of the epitaxial 3R CuSCN film. (A) Optical image of the CuSCN film on 2 inch-diameter Au(111)/Si(111) wafer. (B) XRD pattern of 3R CuSCN(003) on Au(111)/Si(111). (C) (200) pole figure of Au(111). (D) (104) pole figure of 3R CuSCN(003). 3R CuSCN was deposited at −0.4 V for 10 min in 20 mM $CuSO_4$, 20 mM EDTA, and 80 mM KSCN at room temperature.

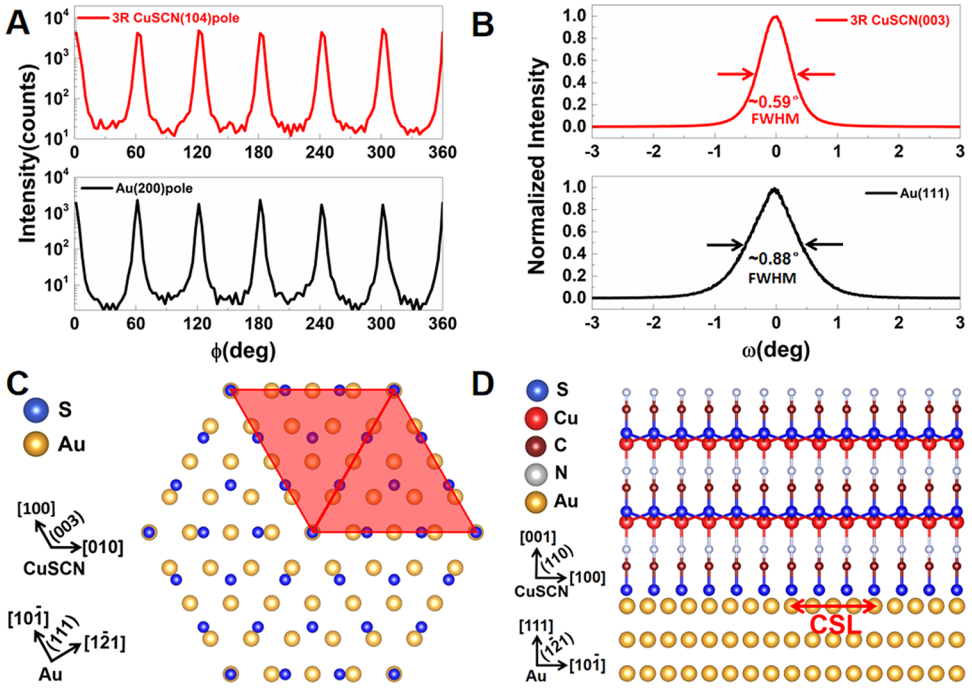

Figure 3. Epitaxial perfection and interface models of 3R CuSCN(003) on a Au(111) substrate. (A) Azimuthal scans of 3R CuSCN(003) at χ = 50.93° and Au(111) at χ = 54.74°. (B) X-ray rocking curves for 3R CuSCN(003) and Au(111). (C) In-plane interface model of S (blue) atoms of 3R CuSCN(003) with Au(111) (orange). 4 S atoms with 5 Au atoms form the coincidence site lattice, which results in a mismatch of +0.22%. (D) Out-of-plane interface model of [001] epitaxial growth of 3R CuSCN(003) on Au(111).

The material deposited positive of C2 grows on top of the adsorbed $Cu(II)_xEDTA_y(SCN)_z$ clusters, which inhibit the epitaxial nucleation on the Au(111) surface. Consistent with this argument, a short nucleation pulse of a Au(111) electrode at −0.4 V for 10 s followed by growth at −0.1 V for 10 min results in epitaxial CuSCN (Figure S4A), whereas a constant potential deposition at −0.1 V for the same time leads to disordered CuSCN (Figure S4B) without clear spots in the (104) pole figure. Therefore, in this work, epitaxial deposition utilizes a constant potential at −0.4 V, and Figure S5 shows a typical current density−time plot.

An optical image of epitaxial CuSCN on a 2 inch-diameter Au(111)/Si(111) wafer is shown in Figure 2A. CuSCN was deposited on a Au(111)/Si(111) wafer with a 28 nm-thick

https://doi.org/10.1021/acs.chemmater.1c02694
Chem. Mater. 2022, 34, 970−978

Au(111) layer that was electrodeposited as reported earlier.[33] Although CuSCN is highly optically transparent, the deposited epitaxial CuSCN film shows a colored appearance due to the Au layer and light wave interference. The orientation of the deposited epitaxial CuSCN on Au(111)/Si(111) was determined by XRD and pole figure measurement. An XRD pattern of CuSCN/Au(111)/Si(111) is shown in Figure 2B. It exhibits the [001] out-of-plane order and is indexed to β-CuSCN. Note that only the {00l} reflections are observed for CuSCN. The sharp peaks for CuSCN are consistent with high crystallinity. It is well known that β-CuSCN exhibits polytypism resulting from different stacking sequences in the [001] direction. AB-type layer stacking corresponds to the hexagonal 2H structure[39] (JCPDS no. 75-2315), whereas the rhombohedral 3R structure[40] (JCPDS no. 29-0581) with the ABC stacking also exists. 3R CuSCN has lattice parameters $a = b = 0.3857$ nm and $c = 1.6449$ nm and $R3m$ (160) space group, whereas 2H CuSCN has lattice parameters $a = b = 0.3850$ nm and $c = 1.0937$ nm and $P6_3mc$ (186) space group. In order to determine the polytype of CuSCN, powder XRD analysis was done, as shown in Figure S6. Powders are scraped from the substrate and ground into micron-size particles. The powder XRD of the CuSCN shows that the material is a pure 3R phase.

The in-plane order of 3R CuSCN(003)/Au(111)/Si(111) was determined using pole figures of crystal planes that are not parallel with the surface. The Au(200) pole (Figure 2C) and Si(220) pole (Figure S7) exhibit six spots (tilt angle: 54.74°) and three spots (tilt angle: 35.5°), respectively, as expected and reported earlier.[33] In the case of CuSCN, the (104) pole figure (Figure 2D) of 3R CuSCN(003) shows six intense spots (tilt angle: 50.93°), which are separated azimuthally by 60°. This tilt angle indicates that the angle between the (003) and (104) planes is 50.93°, consistent with the simulated stereographic projection for 3R CuSCN(003) (Figure S8A). Six spots of 3R CuSCN indicate the existence of parallel and antiparallel orientations. Unlike the simulated stereographic projection in Figure S8B, 3R CuSCN does not have spots at χ of 58.73° in the H(102) pole (Figure S9). This indicates that there is no epitaxial 2H phase, consistent with the powder XRD analysis. To further confirm that the orientation of CuSCN is directly controlled by the Au substrate, we electrodeposited CuSCN on a sputtered Au(111)/glass without in-plane order (Figure S10). The ring pattern in the (104) pole of 3R CuSCN (Figure S10A) grown on Au(111) on glass (Figure S10B) confirms the lack of in-plane order of CuSCN. Hence, the Au(111)/Si(111) substrate directly controls the in-plane orientation of the deposited CuSCN. Therefore, the 3R CuSCN(003) film grows epitaxially on Au(111)/Si(111), and the epitaxial relationship is 3R CuSCN(003)[100]//Au(111)[10$\bar{1}$]//Si(111)[10$\bar{1}$].

The epitaxial perfection of the 3R CuSCN(003) film was further measured. Azimuthal scans were performed for the (104) pole of 3R CuSCN(003) (tilt angle: 50.93°) and the (200) pole of the Au(111) substrate (tilt angle: 54.74°) (Figure 3A). We observe six peaks for both CuSCN and Au, in agreement with pole figure results, corresponding to in-plane parallel and antiparallel domains. The obtained peak/background ratio is 250:1, which confirms a high degree of in-plane order. Rocking curves on 3R CuSCN(003) and Au(111) were done to measure the mosaic spread of CuSCN (Figure 3B). The FWHM (full width at half maximum) were 0.59° for 3R CuSCN(003) and 0.88° for Au(111). The FWHM of 3R CuSCN indicates that the mosaic spread in 3R CuSCN is less than that of the Au(111) substrate.

Interface models of the 3R CuSCN(003) film on the Au(111) substrate are exhibited in Figure 3C,D. In the in-plane interface model (Figure 3C) of S atoms with Au(111), Au and S atoms are colored orange and blue, respectively. By the formation of the CSL, in which 4 S atoms align with 5 Au atoms, a mismatch of +0.22% is produced. Antiparallel and parallel domains could both be observed due to rotational twinning. In the out-of-plane interface model (Figure 3D) showing the cross-sectional structure of CuSCN on Au(111), we could observe that the head-tail direction of linear SCN^- ions is parallel with the [001] growth direction.

The morphological features of the 3R CuSCN(003) were determined by SEM and TEM. Plan-view SEM images of electrodeposited 3R CuSCN(003) on Au(111)/Si(111) are shown in Figure 4A,B. In Figure 4A, after deposition for 60 s,

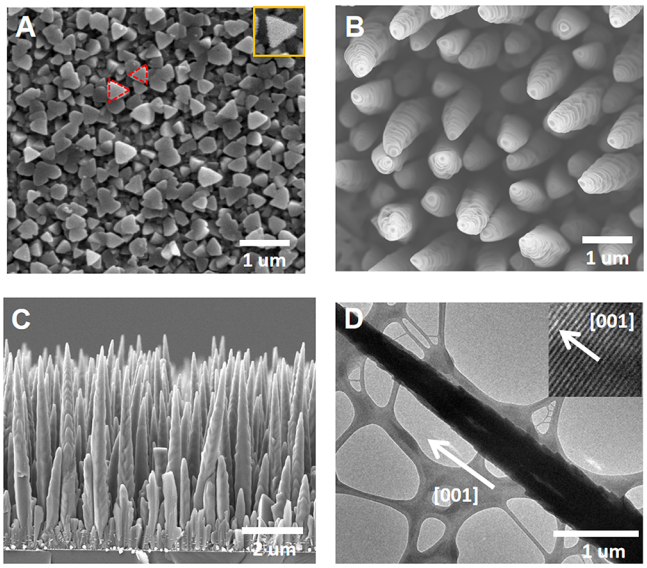

Figure 4. SEM and TEM images of epitaxial 3R CuSCN(003) on Au(111)/Si(111). (A) SEM image (plan-view) of the initial 3R CuSCN(003) after 1 min deposition with 250 nm thickness. (B) SEM image (plan-view) of 3R CuSCN(003) nanorods after 10 min deposition. (C) SEM image (cross-sectional view) of 3R CuSCN(003) nanorods after 10 min deposition. (D) TEM image of a single 3R CuSCN(003) nanorod and HRTEM image showing 0.28 nm interplanar distance. 3R CuSCN was deposited at −0.4 V in 20 mM $CuSO_4$, 20 mM EDTA, and 80 mM KSCN at room temperature.

the initial triangular crystals with an average size 300−500 nm were formed as a homogeneous seed layer with a 250 nm thickness. The high in-plane order in the image is consistent with the epitaxy of 3R CuSCN(003) on the Au(111)/Si(111). Parallel and antiparallel crystals indicate parallel and antiparallel in-plane orientations, consistent with the pole figure results. CuSCN nanorods with 500−800 nm diameters further grow after deposition for 10 min, as shown in Figure 4B. The SEM cross section (Figure 4C) of 3R CuSCN(003) shows that the nanorods are dense and vertical to the Au(111)/Si(111) substrate, indicating the preferred [001] orientation. The nanorod formation mechanism was studied. As shown in Figure S11, when the growth potential of CuSCN is changed from +0.3 to +0.2 V, which corresponds, respectively, to activation control and mass-transport-limited control in the LSV in Figure 1A, the morphology changes from the flat film with uniform triangular crystals (Figure S11A) to

https://doi.org/10.1021/acs.chemmater.1c02694
Chem. Mater. 2022, 34, 970−978

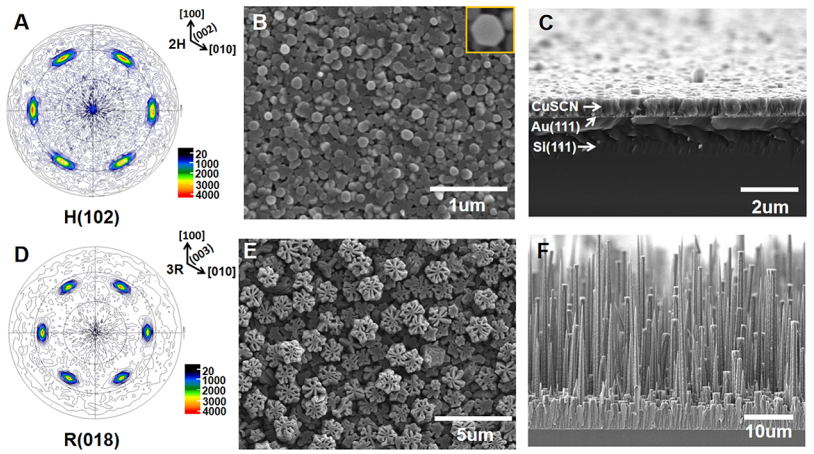

Figure 5. Epitaxial CuSCN with mixed hexagonal and rhombohedral phases. (A) H(102) pole figure for 2H&3R CuSCN. (B) SEM image (plan-view) of 2H&3R CuSCN after 2 min deposition. (C) SEM image (cross-sectional view) of 2H&3R CuSCN after 2 min deposition with 500 nm thickness. (D) R(104) pole figure for 2H&3R CuSCN. (E) SEM image (plan-view) of 2H&3R CuSCN after 15 min deposition. (F) SEM image (cross-sectional view) of 2H&3R CuSCN after 15 min deposition. 2H&3R CuSCN was deposited at −0.4 V in 20 mM $CuSO_4$, 20 mM EDTA, and 40 mM KSCN at room temperature.

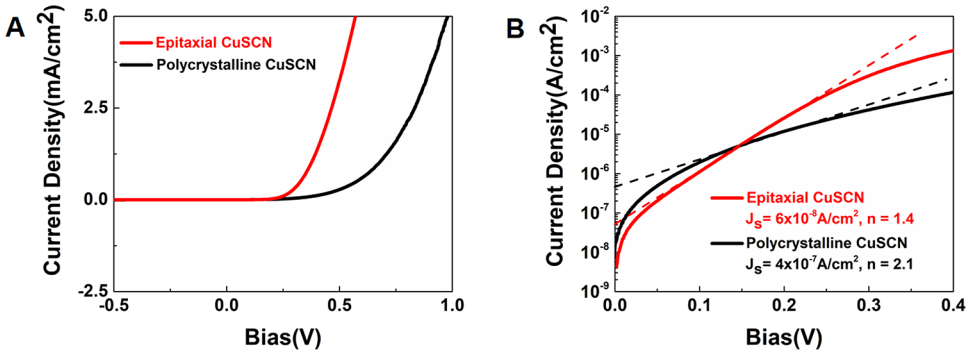

Figure 6. Electronic properties of epitaxial 2H&3R CuSCN. (A) Current density−potential (J−V) plot of Au/CuSCN/Ag diodes. (B) log(J)−V plot to measure the diode quality factor (n) and dark saturation current density (J_s). Epitaxial and polycrystalline CuSCN flat films were deposited at −0.4 and +0.2 V in 20 mM $CuSO_4$, 20 mM EDTA, and 40 mM KSCN at room temperature. The two CuSCN deposits have a constant charge density (0.2 C/cm^2) to maintain similar thicknesses (1.2 μm).

the initial nanorods (Figure S11B) and then to disordered long nanorods (Figure S11C). This shows that the nanorod morphology is due to the limitation of mass transport, in agreement with a previous report.[22] To further gain insights into the atomic arrangement of 3R CuSCN(003), we performed TEM analysis of a single nanorod in Figure 4D. The high-resolution TEM image indicated that the nanorod grows along the [001] direction, and lattice fringes with 0.28 nm interplanar distance match the (006) planes of 3R CuSCN.[41]

Although the 3R CuSCN rods are epitaxial, they lack a continuous film underneath the rods, which may cause leakage or short circuits in electronic devices. Therefore, we developed another continuous epitaxial CuSCN with mixed hexagonal and rhombohedral phases (2H&3R CuSCN) when deposited from a bath with Cu^{2+}/SCN^- = 1/2. The orientations of the 2H&3R CuSCN film are measured by XRD patterns and pole figure analysis. As shown in Figure S12, 2H&3R CuSCN has a [001] orientation that is highly overlapped with 2H and 3R CuSCN. In order to distinguish and quantify compositions of the 2H phase and 3R phases, we did powder XRD analysis of 2H&3R CuSCN. Figure S13 shows mixed peaks for 2H and 3R CuSCN, which confirms the existence of two crystal structures of CuSCN in this work. Rietveld refinement of the diffraction pattern gave 53% hexagonal phase and 47% rhombohedral phase (Rwp 7.0%). As for the in-plane orientation, 2H&3R CuSCN has six intense spots in both H(102) at χ = 58.73° (Figure 5A) and R(104) at χ = 50.93° (Figure 5D) at the same azimuthal angle, indicating that both 2H and 3R phases are epitaxial. The out-of-plane interface model of the 2H phase/Au(111) and the 3R phase/Au(111) is shown in Figure S14. SEM was used to characterize the morphology of 2H&3R CuSCN. After deposition for 2 min, the initial 100−200 nm hexagonal crystals (Figure 5B) form a compact dense film with a thickness of 500 nm (Figure 5C). The further growth of CuSCN for 15 min exhibits a unique morphology with a dense film (5 μm thickness) near the Au surface and ordered hexagonal microrods (1−2 μm diameter, 20−40 μm length) vertical to the substrate (Figure 5E,F) with a snowflake-like surface, which is possibly due to the competition of 2H and 3R phase growth. The microrod morphology with a large surface area could be favorable for efficient charge transport in various devices. The reason for the effect of the Cu^{2+}/SCN^- ion ratio on the crystal structure of CuSCN is still unclear. A possible hypothesis could be that excess SCN^- ions in solution partially substitute the coordination of Cu(II) with EDTA and further form the Cu(II)EDTA$(SCN)_x$ complex. The complex could be

https://doi.org/10.1021/acs.chemmater.1c02694
Chem. Mater. 2022, 34, 970−978

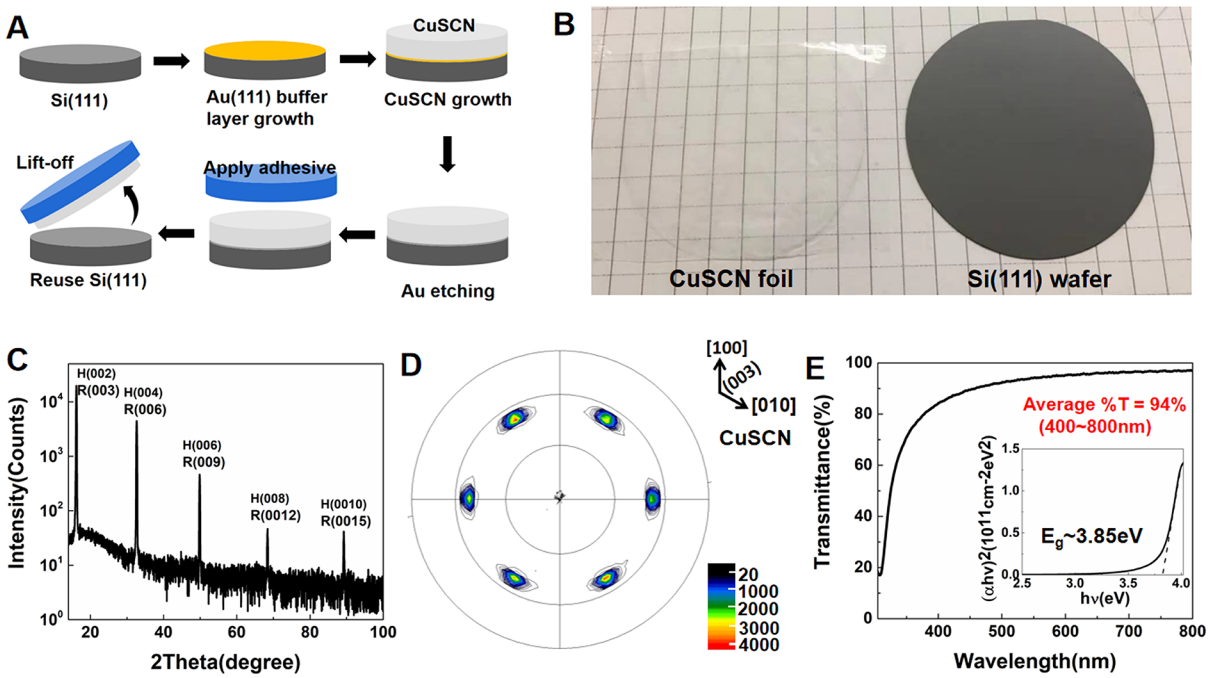

Figure 7. Epitaxial lift-off of highly ordered 2H&3R CuSCN transparent foils. (A) Schematic for epitaxial lift-off 2H&3R CuSCN foil: growth of CuSCN on Au/Si and the following Au etching by KI/I_2 solution produce flexible CuSCN foil, which could be detached by commercial tape. (B) Photograph of transparent, highly ordered 2H&3R CuSCN (2 inch diameter) foil with 400 nm thickness. (C) X-ray diffraction pattern of 2H&3R CuSCN foil. (D) R(104) pole figure of 2H&3R CuSCN foil. (E) UV−vis transmittance spectra of 400 nm 2H&3R CuSCN foil showing average 94% transmittance in the 400−800 nm visible range and Tauc plot showing a 3.85 eV direct bandgap.

absorbed on the surface of CuSCN in a specific posture with the low steric hindrance. Then, the complex is reduced to CuSCN by releasing EDTA and SCN^-. The specific posture causes the Cu−S bond to rotate 120° each time and form 3R packing sequences.

The electronic properties of the epitaxial CuSCN were explored by preparing an inorganic heterojunction (Au/CuSCN/Ag). A 2H&3R CuSCN thin flat film with dense and uniform morphology was chosen for fabrication of the diode. The diode was prepared by coating Ag paste on CuSCN to make a rectifying contact (Figure S15A), while Au(111) forms an ohmic contact (Figure S15B).[42] Epitaxial and polycrystalline CuSCN flat films were electrodeposited with the same charge density (0.2 C/cm^2) to maintain similar thicknesses (1.2 μm), as shown in Figure S16A,B, respectively. The cross-sectional SEM images of the Au/epitaxial CuSCN/Ag diode and Au/polycrystalline CuSCN/Ag diode are shown in Figure S16C,D. The $J-V$ response of Au/epitaxial CuSCN/Ag exhibits a more significant rectifying behavior (Figure 6A). The diode quality factor, n, was used to determine the quality of the rectifying behavior. An ideal diode has $n = 1.0$. In Figure 6B, the epitaxial CuSCN has a diode quality factor of 1.4, whereas a diode produced with polycrystalline CuSCN has a diode quality factor of 2.1. A smaller diode quality factor for epitaxial CuSCN indicates that epitaxy of CuSCN is beneficial to suppressing carrier recombination. The high order and lack of grain boundaries of epitaxial CuSCN could also improve carrier mobility, which is favorable to various electronic devices such as perovskite solar cells.

The schematic for epitaxial lift-off of 2H&3R CuSCN foil is shown in Figure 7A. A flat epitaxial 2H&3R CuSCN film (Figure 5C) grows initially on the Au buffer layer on the Si wafer. Au can then be etched in KI/I_2 for effortless lift-off by commercial adhesive tape. Si could be reusable after each fabrication cycle. It is unexpected that CuSCN could resist the oxidization of KI/I_2 because KI/I_2 is a strong oxidant that could oxidize Cu^+ to Cu(II). The result confirms the exceptional chemical stability of CuSCN. Figure 7B shows the photograph of a continuous transparent 2H&3R CuSCN foil with a thickness of 400 nm. The out-of-plane order of the 2H&3R CuSCN foil was confirmed by the XRD pattern in Figure 7C, which only exhibits the {001} family of peaks. The in-plane order was demonstrated by an R(104) pole figure, which has six spots (tilt angle: 50.93°) separated azimuthally by 60° (Figure 7D). Hence, the 2H&3R CuSCN foil remains highly ordered after Au etching. Figure 7E shows the optical transparency of the 400 nm-thick 2H&3R CuSCN foil. The transmittance spectrum shows 94% average transmittance in the visible range (400−800 nm). The Tauc plot in Figure 7E shows a 3.85 eV direct band gap, which is exceptionally large compared with other Cu(I)-based p-type semiconductors. The surface of 2H&3R CuSCN foil remained continuous and featureless without cracks after 1000 bending cycles (Figure S17). The highly ordered 2H&3R CuSCN foil could form the basis of future transparent and flexible electronics.

CONCLUSIONS

We demonstrate an electrochemical method for depositing epitaxial hole transport CuSCN nanorods with a [001] orientation on the Au(111) surface. CuSCN with the pure 3R structure and 2H & 3R mixture were produced by adjusting the Cu^{2+}/SCN^- ratio in the deposition solution. Epitaxial CuSCN/Au forms an ideal HTM/metal system for various opto-electronic devices. Here, a diode is produced by forming the Au/epitaxial CuSCN/Ag heterojunction. This work also opens interesting avenues for other epitaxial hole transport layers such as NiO and $CuAlO_2$. Good chemical stability of

https://doi.org/10.1021/acs.chemmater.1c02694
Chem. Mater. 2022, 34, 970−978

CuSCN allows Au etching and epitaxial lift-off to produce a CuSCN foil with high optical transparency and large bandgap. The highly ordered 2H&3R CuSCN foil has possible applications such as an efficient HTM in perovskite solar cells via a dry-transfer method and flexible transparent electrodes. It could also serve as a basis for future flexible and transparent electronic devices. This Au etching method shown here could be a general way to produce various flexible ceramic foils grown on a Au substrate, such as Bi_2O_3 and PbO_2.

MATERIALS AND METHODS

Si Wafer Processing for Au Deposition. Si(111) wafers (phosphorus-doped, N-type, 0.1−2.0 Ω·cm, Virginia Semiconductor Inc.) were used in this work. RCA procedures were applied to completely remove organic/inorganic impurities on the Si surface. In/Ga alloy was coated on the back of the wafers, and then a silver wire was attached by silver paste to achieve good electrical contact. In order to prevent electrodeposition on the back, an insulating layer of Apiezon Type W wax was coated and fully dried. Before use, a hydrogen-terminated Si surface was produced by washing wafers with dilute (5%) hydrofluoric acid solution for 30−45 s at room temperature. The Au(111) deposition process (using an Autolab 30 potentiostat) followed our previous report in a three-electrode system using Si as a working electrode.[33] The epitaxial Au(111) films were grown to a thickness of 28 nm.

Electrodeposition of CuSCN and Foil Fabrication. Electrodeposition of rod-like CuSCN was performed in an aqueous $CuSO_4$-EDTA-KSCN system as previously reported.[17,18,23] The solution was prepared by dissolving 20 mM $Cu(SO_4)\cdot 5H_2O$, 20 mM ethylenediaminetetraacetic acid (EDTA), and various concentrations of KSCN. The concentrations of KSCN for 3R CuSCN and 2H&3R CuSCN were 80 and 40 mM, respectively. CuSCN films were electrodeposited at a constant potential at −0.4 V on the Au(111)/Si(111) substrate with 300 rpm stirring. A CuSCN foil was produced by immersion in aqueous 0.3 M I_2 and 0.6 M KI solution for 60 s to completely etch the Au layer. The CuSCN foil was detached from the Si substrate by commercial (3 M) adhesive tape.

Electrochemical Analysis. LSVs were acquired on an Autolab 30 potentiostat using a Au RDE (3 mm diameter) at 1000 rpm rotation rate. The potential scan rate was 10 mV/s, and the step size was 1 mV.

Diode Fabrication. Au/CuSCN/Ag was fabricated by coating silver print II (GC electronics) on CuSCN/Au/Si. Silver wires were then connected to the silver print and the Au surface, respectively. The values of the Au/CuSCN/Ag diode factor were determined by devices with the same area of 0.25 cm^2.

X-ray Diffraction, SEM, and TEM Measurements. X-ray diffraction patterns, pole figures, and azimuthal scans were run on a high-resolution Philips X'Pert Materials Research diffractometer using the accessories and procedures outlined in our previous report.[43] SEM was done on a FEI Helios Nanolab microscope, and TEM was done on a FEI Tecnai F20 microscope.

ASSOCIATED CONTENT

Supporting Information

The Supporting Information is available free of charge at https://pubs.acs.org/doi/10.1021/acs.chemmater.1c02694.

Powder XRD pattern of spontaneous precipitation in the $CuSO_4$-KSCN bath, deposited CuSCN in the $CuSO_4$-KSCN bath, analysis of polycrystalline CuSCN with a slightly preferred [001] orientation, pulse deposition analysis, current density−time plot, phase analysis of 3R CuSCN powder, (220) pole figure of Si(111), calculated stereographic projections for CuSCN, H(102) pole figure for 3R CuSCN(003), pole figures for CuSCN on the textured Au(111) substrate, CuSCN nanorod formation due to mass transport limitation, XRD of the 2H&3R CuSCN film, phase analysis of 2H&3R CuSCN powder, out-of-plane interface model of 3R CuSCN/Au and 2H CuSCN/Au, $J-V$ plot of Ag/CuSCN/Ag and Au/CuSCN/Au&Pd, cross-sectional SEM image of Au/CuSCN/Ag diodes, and SEM image of the CuSCN foil after bending 1000 times (PDF)

AUTHOR INFORMATION

Corresponding Author

Jay A. Switzer − *Department of Chemistry and Graduate Center for Materials Research, Missouri University of Science and Technology, Rolla, Missouri 65409-1170, United States;* orcid.org/0000-0002-7332-4634; Email: jswitzer@mst.edu

Authors

Bin Luo − *Department of Chemistry and Graduate Center for Materials Research, Missouri University of Science and Technology, Rolla, Missouri 65409-1170, United States;* orcid.org/0000-0002-8996-1734

Avishek Banik − *Department of Chemistry and Graduate Center for Materials Research, Missouri University of Science and Technology, Rolla, Missouri 65409-1170, United States;* orcid.org/0000-0001-7269-1929

Eric W. Bohannan − *Department of Chemistry and Graduate Center for Materials Research, Missouri University of Science and Technology, Rolla, Missouri 65409-1170, United States*

Complete contact information is available at: https://pubs.acs.org/10.1021/acs.chemmater.1c02694

Notes

The authors declare no competing financial interest.

ACKNOWLEDGMENTS

This material is based on work supported by the U.S. Department of Energy, Office of Basic Energy Sciences, Division of Materials Sciences and Engineering, under grant no. DE-FG02-08ER46518.

REFERENCES

(1) Matsushima, T.; Bencheikh, F.; Komino, T.; Leyden, M. R.; Sandanayaka, A. S. D.; Qin, C.; Adachi, C. High Performance from Extraordinarily Thick Organic Light-Emitting Diodes. *Nature* **2019**, *572*, 502−506.

(2) Burschka, J.; Pellet, N.; Moon, S. J.; Humphry-Baker, R.; Gao, P.; Nazeeruddin, M. K.; Grätzel, M. Sequential Deposition as a Route to High-Performance Perovskite-Sensitized Solar Cells. *Nature* **2013**, *499*, 316−319.

(3) Abdi-Jalebi, M.; Dar, M. I.; Senanayak, S. P.; Sadhanala, A.; Andaji-Garmaroudi, Z.; Pazos-Outón, L. M.; Friend, R. H. Charge Extraction via Graded Doping of Hole Transport Layers Gives Highly Luminescent and Stable Metal Halide Perovskite Devices. *Sci. Adv.* **2019**, *5*, No. eaav2012.

(4) Arora, N.; Dar, M. I.; Hinderhofer, A.; Pellet, N.; Schreiber, F.; Zakeeruddin, S. M.; Grätzel, M. Perovskite Solar Cells with CuSCN Hole Extraction Layers Yield Stabilized Efficiencies Greater than 20%. *Science* **2017**, *358*, 768−771.

(5) Pan, L.; Liu, Y.; Yao, L.; Ren, D.; Sivula, K.; Grätzel, M.; Hagfeldt, A. Cu_2O Photocathodes with Band-tail States Assisted Hole Transport for Standalone Solar Water Splitting. *Nat. Commun.* **2020**, *11*, 1−10.

(6) Perumal, A.; Faber, H.; Yaacobi-Gross, N.; Pattanasattayavong, P.; Burgess, C.; Jha, S.; McLachlan, M. A.; Stavrinou, P. N.; Anthopoulos, T. D.; Bradley, D. D. High-efficiency, Solution-

processed, Multilayer Phosphorescent Organic Light-emitting Diodes with A Copper Thiocyanate Hole-injection/Hole-transport Layer. *Adv. Mater.* **2015**, *27*, 93−100.
(7) Chavhan, S. D.; Ou, T. H.; Jiang, M. R.; Wang, C. W.; Jou, J. H. Enabling High-efficiency Organic Light-emitting Diode with Trifunctional Solution-processable Copper(I) Thiocyanate. *J. Phys. Chem. C* **2018**, *122*, 18836−18840.
(8) Xu, L. J.; Wang, J. Y.; Zhu, X. F.; Zeng, X. C.; Chen, Z. N. Phosphorescent Cationic Au_4Ag_2 Alkynyl Cluster Complexes for Efficient Solution-Processed Organic Light-Emitting Diodes. *Adv. Funct. Mater.* **2015**, *25*, 3033−3042.
(9) Pattanasattayavong, P.; Yaacobi-Gross, N.; Zhao, K.; Ndjawa, G. O. N.; Li, J.; Yan, F.; O'regan, B. C.; Amassian, A.; Anthopoulos, T. D. Hole-transporting Transistors and Circuits Based on the Transparent Inorganic Semiconductor Copper (I) Thiocyanate (CuSCN) Processed from Solution at Room Temperature. *Adv. Mater.* **2013**, *25*, 1504−1509.
(10) Baig, S.; Hendsbee, A. D.; Kumar, P.; Ahmed, S.; Li, Y. Yttrium-doped CuSCN Thin Film Transistor: Synthesis and Optoelectronic Characterization Study. *J. Mater. Chem. C* **2019**, *7*, 14543−14554.
(11) Wijeyasinghe, N.; Eisner, F.; Tsetseris, L.; Lin, Y. H.; Seitkhan, A.; Li, J.; Yan, F.; Solomeshch, O.; Tessler, N.; Patsalas, P.; Anthopoulos, T. D. P-Doping of Copper (I) Thiocyanate (CuSCN) Hole-Transport Layers for High-Performance Transistors and Organic Solar Cells. *Adv. Funct. Mater.* **2018**, *28*, 1802055.
(12) Wijeyasinghe, N.; Regoutz, A.; Eisner, F.; Du, T.; Tsetseris, L.; Lin, Y. H.; Anthopoulos, T. D. Copper (I) Thiocyanate (CuSCN) Hole-transport Layers Processed from Aqueous Precursor Solutions and Their Application in Thin-film Transistors and Highly Efficient Organic and Organometal Halide Perovskite Solar Cells. *Adv. Funct. Mater.* **2017**, *27*, 1710418.
(13) Sajjad, M. T.; Park, J.; Gaboriau, D.; Harwell, J. R.; Odobel, F.; Reiss, P.; Samul, I. D. W.; Aldakov, D. CuSCN Nanowires as Electrodes for p-Type Quantum Dot Sensitized Solar Cells: Charge Transfer Dynamics and Alumina Passivation. *J. Phys. Chem. C* **2018**, *122*, 5161−5170.
(14) Gottam, S. R.; Tsai, C. T.; Wang, L. W.; Li, C. Y.; Lin, C. C.; Chu, S. Y. Communication-Pseudohalide β-CuSCN Nanorod-Based Thin Film as a Potential Hydrogen Gas Sensor. *J. Electrochem. Soc.* **2020**, *167*, No. 027513.
(15) Wang, F.; Chen, D.; Hu, Z.; Qin, L.; Sun, X.; Huang, Y. In Situ Decoration of CuSCN Nanorod Arrays with Carbon Quantum Dots for Highly Efficient Photoelectrochemical Performance. *Carbon* **2017**, *125*, 344−351.
(16) Yaacobi-Gross, N.; Treat, N. D.; Pattanasattayavong, P.; Faber, H.; Perumal, A. K.; Stingelin, N.; Bradley, D. D. C.; Stavrinou, P. N.; Heeney, M.; Anthopoulos, T. D. High-Efficiency Organic Photovoltaic Cells Based on the Solution-Processable Hole Transporting Interlayer Copper Thiocyanate (CuSCN) as a Replacement for PEDOT: PSS. *Adv. Energy Mater.* **2015**, *5*, 1401529.
(17) Wu, W.; Jin, Z.; Hua, Z.; Fu, Y.; Qiu, J. Growth Mechanisms of CuSCN Films Electrodeposited on ITO in EDTA-chelated Copper (II) and KSCN Aqueous Solution. *Electrochim. Acta* **2005**, *50*, 2343−2349.
(18) Ramírez, D.; Álvarez, K.; Riveros, G.; González, B.; Dalchiele, E. A. Electrodeposition of CuSCN Seed Layers and Nanowires: A Microelectrogravimetric Approach. *Electrochim. Acta* **2017**, *228*, 308−318.
(19) Liu, C.; Wu, W.; Liu, K.; Li, M.; Hu, G.; Xu, H. Orientation Growth and Electrical Property of CuSCN Films Associated with the Surface States. *CrystEngComm* **2012**, *14*, 6750−6754.
(20) Sankapal, B. R.; Goncalves, E.; Ennaoui, A.; Lux-Steiner, M. C. Wide Band Gap P-type Windows by CBD and SILAR Methods. *Thin Solid Films* **2004**, *451*, 128−132.
(21) Cheng, B.; Zhao, J.; Xiao, L.; Cai, Q.; Guo, R.; Xiao, Y.; Lei, S. PMMA Interlayer-modulated Memory Effects by Space Charge Polarization in Resistive Switching Based on CuSCN-nanopyramids/ZnO-nanorods P-N Heterojunction. *Sci. Rep.* **2015**, *5*, 1−9.
(22) Sun, L.; Ichinose, K.; Sekiya, T.; Sugiura, T.; Yoshida, T. Cathodic Electrodeposition of P-CuSCN Nanorod and Its Dye-sensitized Photocathodic Property. *Phys. Procedia* **2011**, *14*, 12−24.
(23) Gan, X.; Zhaohui, W.; Liu, K.; Du, X.; Guo, L.; Liu, H. Electrochemical Deposition of CuSCN Nanorod Arrays by Using EDTA as Chelating Agent. *J. Nanosci. Nanotechnol.* **2017**, *17*, 538−543.
(24) Iwamoto, T.; Ogawa, Y.; Sun, L.; White, M. S.; Glowacki, E. D.; Scharber, M. C.; Saracific, N. S.; Manseki, K.; Sugiura, T.; Yoshida, T. Electrochemical Self-assembly of Nanostructured CuSCN/rhodamine B Hybrid Thin Film and Its Dye-sensitized Photocathodic Properties. *J. Phys. Chem. C* **2014**, *118*, 16581−16590.
(25) Lin, H. P.; Lin, X. J.; Perng, D. C. Electrodeposited CuSCN Metal-semiconductor-metal High Performance Deep-ultraviolet Photodetector. *Appl. Phys. Lett.* **2018**, *112*, No. 021107.
(26) Xi, Q.; Gao, G.; Zhou, H.; Zhao, Y.; Wu, C.; Wang, L.; Guo, P.; Xu, J. Highly Efficient Inverted Solar Cells Based on Perovskite Grown Nanostructures Mediated by CuSCN. *Nanoscale* **2017**, *9*, 6136−6144.
(27) Pattanasattayavong, P.; Promarak, V.; Anthopoulos, T. D. Electronic Properties of Copper (I) Thiocyanate (CuSCN). *Adv. Electron. Mater.* **2017**, *3*, 1600378.
(28) Luo, W.; Zeng, C.; Du, X.; Leng, C.; Yao, W.; Shi, H.; Wei, X.; Du, C.; Lu, S. Copper Thiocyanate/Copper Iodide Based Hole Transport Composites with Balanced Properties for Efficient Polymer Light-Emitting Diodes. *J. Mater. Chem. C* **2018**, *6*, 4895−4902.
(29) Shan, F.; Liu, A.; Zhu, H.; Kong, W.; Liu, J.; Shin, B.; Fortunato, E.; Martins, R.; Liu, G. High-mobility P-type NiOx Thin-film Transistors Processed at Low Temperatures with Al_2O_3 High-k Dielectric. *J. Mater. Chem. C* **2016**, *4*, 9438−9444.
(30) Shi, D.; Qin, X.; Li, Y.; He, Y.; Zhong, C.; Pan, J.; Dong, H.; Xu, W.; Li, T.; Hu, W.; Brédas, J.-L.; Bakr, O. M. Spiro-OMeTAD Single Crystals: Remarkably Enhanced Charge-carrier Transport via Mesoscale Ordering. *Sci. Adv.* **2016**, *2*, No. e1501491.
(31) Hatch, S. M.; Briscoe, J.; Dunn, S. A Self-powered ZnO-nanorod/CuSCN UV Photodetector Exhibiting Rapid Response. *Adv. Mater.* **2013**, *25*, 867−871.
(32) Switzer, J. A.; Shumsky, M. G.; Bohannan, E. W.; Crystals, E. C. S. *Science* **1999**, *284*, 293−296.
(33) Mahenderkar, N. K.; Chen, Q.; Liu, Y. C.; Duchild, A. R.; Hofheins, S.; Chason, E.; Switzer, J. A. Epitaxial Lift-off of Electrodeposited Single-crystal Gold Foils for Flexible Electronics. *Science* **2017**, *355*, 1203−1206.
(34) Banik, A.; Tubbesing, J. Z.; Luo, B.; Zhang, X.; Switzer, J. A. Epitaxial Electrodeposition of Optically Transparent Hole-Conducting CuI on n-Si (111). *Chem. Mater.* **2021**, *33*, 3220−3227.
(35) Petti, L.; Pattanasattayavong, P.; Lin, Y. H.; Münzenrieder, N.; Cantarella, G.; Yaacobi-Gross, N.; Anthopoulos, T. D. Solution-processed P-type Copper (I) Thiocyanate (CuSCN) for Low-voltage Flexible Thin-film Transistors and Integrated Inverter Circuits. *Appl. Phys. Lett.* **2017**, *110*, 113504.
(36) Fernando, C. A. N.; Kumarawadu, I.; Takahashi, K.; Kitagawa, A.; Suzuki, M. Crystal Violet Dye-sensitized Photocurrent by Participation of Surface States on P-CuSCN Photocathode. *Sol. Energy Mater. Sol. Cells* **1999**, *58*, 337−347.
(37) Li, X.; Gewirth, A. A. Potential-Dependent Reorientation of Thiocyanate on Au Electrodes. *J. Am. Chem. Soc.* **2003**, *125*, 11674−11683.
(38) Chappaz-Gillot, C.; Salazar, R.; Berson, S.; Ivanova, V. Insights into CuSCN Nanowire Electrodeposition on Flexible Substrates. *Electrochim. Acta* **2013**, *110*, 375−381.
(39) Smith, D. L.; Saunders, V. I. Preparation and Structure Refinement of the 2H polytype of β-Copper (I) Thiocyanate. *Acta Crystallogr. B* **1982**, *38*, 907−909.
(40) Smith, D. L.; Saunders, V. I. The Structure and Polytypism of the β Modification of Copper (I) Thiocyanate. *Acta Crystallogr. B* **1981**, *37*, 1807−1812.
(41) Li, L.; Liang, J.; Qin, L.; Chen, D.; Huang, Y. In Situ Growth of a P-type CuSCN/Cu_2O Heterojunction to Enhance Charge Trans-

port and Suppress Charge Recombination. *J. Mater. Chem. C* **2019**, *7*, 6872−6878.
(42) Wyatt-Moon, G.; Georgiadou, D. G.; Semple, J.; Anthopoulos, T. D. Deep Ultraviolet Copper (I) Thiocyanate (CuSCN) Photodetectors Based on Coplanar Nanogap Electrodes Fabricated via Adhesion Lithography. *ACS Appl. Mater. Interfaces* **2017**, *9*, 41965−41972.
(43) Luo, B.; Banik, A.; Bohannan, E. W.; Switzer, J. A. Epitaxial Electrodeposition of Cu(111) onto an l-Cysteine Self-Assembled Monolayer on Au(111) and Epitaxial Lift-Off of Single-Crystal-like Cu Foils for Flexible Electronics. *J. Phys. Chem. C* **2020**, *124*, 21426−21434.

https://doi.org/10.1021/acs.chemmater.1c02694
Chem. Mater. 2022, 34, 970−978